Microscopy, 2022, **00(00)**, 1–7
DOI: https://doi.org/10.1093/jmicro/dfac057
Advance Access Publication Date: 2 November 2022
Article

MICROSCOPY

Hybrid mode atomic force microscopy of phase modulation and frequency modulation

Tatsuya Yamamoto[1], Masato Miyazaki[1], Hikaru Nomura[2], Yan Jun Li[1] and Yasuhiro Sugawara[1,*]

[1]Department of Applied Physics, Graduate School of Engineering, Osaka University, 2-1 Yamada-oka, Suita, Osaka 565-0871, Japan
[2]Department of Materials Engineering Science, Graduate School of Engineering Science, Osaka University, 1-3 Yachinake-yama, Toyonaka, Osaka 560-0043, Japan
*To whom correspondence should be addressed. E-mail: sugawara@ap.eng.osaka-u.ac.jp

Abstract

We propose hybrid phase modulation (PM)/frequency modulation (FM) atomic force microscopy (AFM) to increase the imaging speed of AFM in high-Q environments. We derive the relationship between the phase shift, the frequency shift and the tip–sample interaction force from the equation of motion for the cantilever in high-Q environments. The tip–sample conservative force is approximately given by the sum of the conservative force with respect to the phase shift in the PM mode and that with respect to the frequency shift in the FM mode. We preliminarily demonstrate that the hybrid PM/FM-AFM is a new and very promising AFM operation mode that can increase imaging speed.

Key words: atomic force microscopy, phase modulation, frequency modulation, hybrid mode

Introduction

Various dynamic processes occur on surfaces, such as surface diffusion, phase transitions, self-organization phenomena, chemical reactions and etching [1]. These dynamic processes are of great fundamental and technological interest. The ability to study these processes with high spatial and high temporal resolutions is expected to provide access to non-equilibrium dynamics at the atomic level. Atomic force microscopy (AFM) enables not only the imaging of atoms and molecules on surfaces with ultimate spatial resolution [2–5] but also manipulation [6,7] and characterization of substances [8,9]. Thus, AFM is now an indispensable nanoscale tool in the study of surfaces. However, the time resolution of AFM systems operating in a vacuum is one of their most severe limitations because the typical image acquisition time is on the order of 10 s or longer. High-speed AFM systems operating in low-Q-factor (Q) environments have been developed [10,11], but not those operating in high-Q environments. Therefore, developing an AFM system capable of high-speed imaging in high-Q environments is one of the most important technical challenges.

AFM systems have three operating modes, namely, amplitude modulation (AM) [10,12,13], frequency modulation (FM) [14–16] and phase modulation (PM) [17–23]. In AM-AFM, a cantilever is always driven at or near the resonance frequency (f_0) with an external oscillator. The tip–sample interaction is measured by the change (ΔA) in oscillating amplitude. In AM-AFM, in which the cantilever is externally driven in the constant-excitation-amplitude (CE) mode, two stable vibration states coexist depending on the driving force and tip–sample distance [24], resulting in complex dynamic behaviors such as hysteresis and bistability [25] due to nonlinearities in the tip–sample interaction force. In addition, in AM-AFM, the time constant τ_{AM} of the transient response of ΔA to a change in force is given by $\tau_{\mathrm{AM}} = 2Q/f_0$, and it becomes longer as Q increases [10]. This makes it impossible to use AM-AFM in a vacuum and also limits the imaging speed in air.

In FM-AFM, a cantilever is always driven at the resonance frequency on the basis of a self-driven oscillator. The tip–sample interaction is measured by the frequency shift (Δf) of the oscillating cantilever. In FM-AFM, the vibration amplitude of the cantilever is mostly kept constant using an automatic gain control circuit. This constant-amplitude (CA) mode can not only prevent the complicated dynamical behaviors, such as hysteresis and bistability, but also enable the measurement of conservative and dissipative interaction forces independently. In FM-AFM, the time constant τ_{FM} of the transient response of Δf to a change in force is given by $\tau_{\mathrm{FM}} = 1/f_0$ and is not affected by the quality factor (Q-factor) of the cantilever. Therefore, an FM-AFM system can be operated in a high-Q environment, such as a vacuum, and can achieve extremely high force sensitivity and spatial resolution. However, τ_{FM} is often substantially longer than this predicted value ($1/f_0$) owing to the delay caused by the self-excitation circuit (i.e. phase feedback loop). This delay is particularly noticeable when the self-excitation circuit includes a phase-locked loop (PLL) circuit with a bandwidth of 1 kHz or less [15]. Thus, the imaging speed is much lower than expected from τ_{FM}.

In PM-AFM, a cantilever is driven at a fixed resonance frequency with an external oscillator. The tip–sample interaction is measured from the phase shift ($\Delta\phi$) of the oscillating cantilever. In PM-AFM operating in the CE mode, complex dynamic behaviors, such as hysteresis and bistability, remain a problem [25]. In PM-AFM operating in the CA mode, in

Received 28 September 2022; Revised 24 October 2022; Editorial Decision 27 October 2022; Accepted 1 November 2022

contrast, such instabilities in non-linear cantilever dynamics can be eliminated and quantitative spectroscopic curves can be obtained for the tip–sample distance [19]. In addition, in PM-AFM, the time constant τ_{PM} of the transient response of $\Delta\phi$ to force changes is given by $\tau_{PM} = 1/f_0$, which is not influenced by the Q-factor of the cantilever. These features suggest that the application of PM-AFM in the CA mode is advantageous for realizing high-speed imaging in high-Q environments, such as a vacuum, as well as in low-Q environments, such as a liquid. So far, the performance of PM-AFM in the CA mode in low-Q environments has been investigated [17–23], but that in the CA mode in high-Q environments has hardly been studied.

In this paper, to increase the imaging speed of AFM systems operating in high-Q environments, we propose a hybrid mode AFM that utilizes the advantages of PM-AFM, i.e. fast transient response, and FM-AFM, i.e. the cantilever is always excited near its resonant frequency. First, we discuss the limitations of PM-AFM operation in high-Q environments. Then, we propose the utilization of the hybrid technique of PM and FM mode operation in high-Q environments to overcome the limitations. We derive the relationship between the phase shift, the frequency shift and the tip–sample interaction force from the equation of motion for the cantilever. We show that the conservative tip–sample interaction force is approximately given by the sum of the conservative interaction force with respect to the phase shift in the PM mode and that with respect to the frequency shift in the FM mode. We preliminarily demonstrate that the hybrid PM/FM-AFM is a new and very promising AFM operation mode that can increase imaging speed.

Hybrid PM/FM mode that overcomes the limitations of PM mode in high-Q environments

We discuss the limitations of the PM mode in high-Q environments and propose the hybrid PM/FM mode for overcoming the limitations. Fig. 1 shows the phases (ϕ) of the oscillating cantilever as a function of driving frequency (f). The resonance frequency at which the phase ϕ is $-\pi/2$ is shifted by the tip–sample interaction. f_0 is the resonance frequency of the cantilever when there is no tip–sample interaction (black line), while f_1 and f_2 are the resonance frequencies of the cantilever when there is tip–sample interaction (red and blue lines, respectively). In PM-AFM, the driving frequency is fixed at or near the resonance frequency f_0 at which the phase is $\phi = -\pi/2$. When the tip–sample interaction force becomes strong, the resonance frequency of the cantilever at which the phase is $\phi = -\pi/2$ changes to $f_1 = f_0 + \Delta f_{01}$, where Δf_{01} is the frequency shift of the cantilever. The tip–sample interaction force is measured from the phase shift ($\Delta\phi_{01}$) of the cantilever at f_0.

The minimum detectable force density of PM-AFM in high-Q environments is given by

$$\delta F_{PM} = \sqrt{\frac{k k_B T}{Q^2}} \tag{1}$$

where k and Q are the spring constant and the natural Q-factor of the cantilever, respectively. k_B and T are the Boltzmann constant and the absolute temperature, respectively.

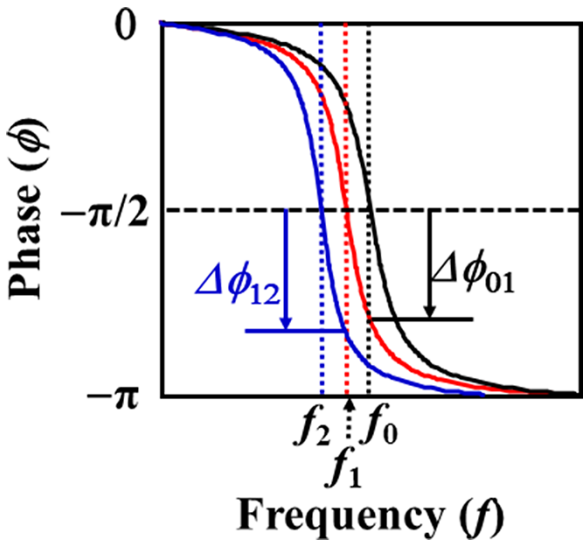

Fig. 1. Phase of the oscillating cantilever as a function of driving frequency. In hybrid PM/FM-AFM, the limitation of the available frequency shift can be solved by changing the driving frequency f_0 to f_1 using the FM mode, and the tip–sample interaction force can be determined from the frequency shift ($f_1 - f_0$) and the phase shift ($\Delta\phi_{12}$) at f_1 using the PM mode.

Here, noise arising from the cantilever deflection sensor is assumed to be much lower than that from the thermal Brownian motion of the cantilever. This equation means that high force sensitivity can be obtained by increasing Q-factor. However, increasing Q-factor has the disadvantage of limiting the available frequency shift Δf_{01} of the cantilever, which is induced by the tip–sample interaction. That is, in PM-AFM, a cantilever is driven at a fixed resonance frequency f_0, and the available frequency shift Δf_{01} must be less than the half width of the resonance peaks of the cantilever,

$$|\Delta f_{01}| < \frac{f_0}{2Q} \tag{2}$$

This condition is easily satisfied in low-Q environments such as in solutions but difficult to satisfy in high-Q environments such as a vacuum. For example, under the typical imaging conditions in a vacuum, for a typical cantilever with $Q = 20\,000$ and $f_0 = 300$ kHz in a vacuum, the maximum available frequency shift $|\Delta f_{01}|$ is only 7.5 Hz, which is unusable for most high-resolution imaging.

One possible way to satisfy the condition of the PM mode in Eq. (2) in high-Q environments is to use hybrid PM/FM-AFM. That is, as shown in Fig. 1, first, the limitation of the available frequency shift is resolved by changing the driving frequency f_0 to f_1 in the FM mode under weak feedback conditions. Second, by measuring the phase shift ($\Delta\phi_{12}$) at f_1 in the PM mode, the interaction force between the tip and sample can be determined from the frequency shift ($\Delta f_{01} = f_1 - f_0$) and the phase shift ($\Delta\phi_{12}$). Hence, the distance between the tip and the sample is controlled by the sum of the feedback signal for the phase shift ($\Delta\phi_{12}$) and the feedback signal for the frequency shift (Δf_{01}). This hybrid PM/FM-AFM has the advantage of increasing the imaging speed because there is no need to wait for the transient response of the frequency shift in PLL as in the case of the FM mode.

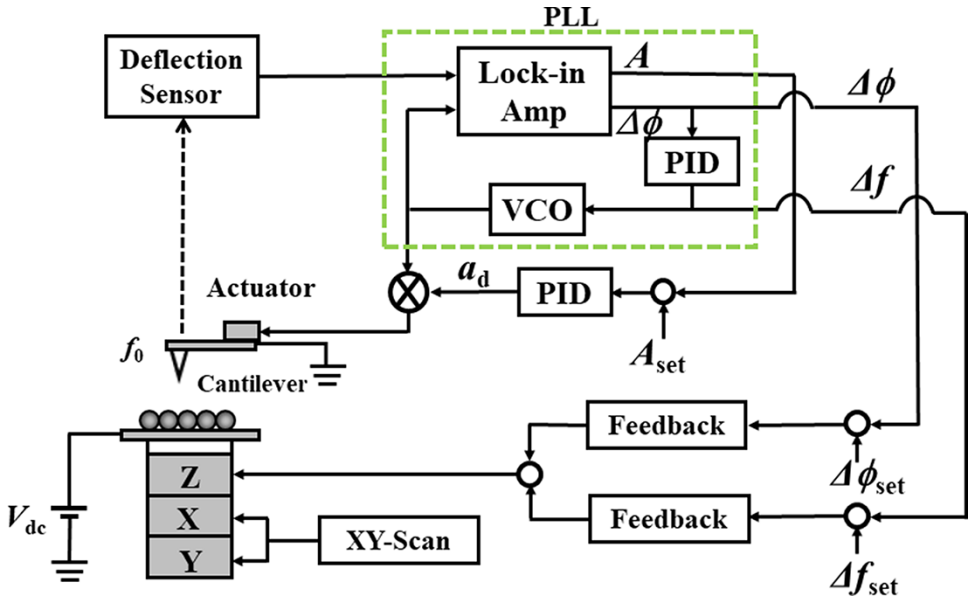

Fig. 2. Block diagram of the hybrid PM/FM-AFM.

Hybrid PM/FM-AFM system

Here, we consider the configuration for realizing a hybrid PM/FM-AFM. Fig. 2 shows a block diagram of the proposed hybrid PM/FM-AFM. Its configuration is very similar to that of FM-AFM that uses a PLL circuit in the self-excitation loop. The cantilever is driven with a voltage-controlled oscillator at a frequency (f). Cantilever deflection is detected with a deflection sensor such as an optical beam deflection sensor. The amplitude A and phase ϕ of the oscillating cantilever are measured with a lock-in amplifier. A phase signal is fed into a proportional–integral–differential controller to control the input voltage of voltage-controlled oscillator, and the frequency shift Δf of the cantilever is measured. The oscillation amplitude A is maintained at a constant value with the automatic gain control circuit using a multiplier and a proportional–integral–differential controller in the CA mode. The frequency shift Δf and the phase shift $\Delta\phi$ are separately connected to feedback circuits, and AFM images are obtained from the sum of these two feedback outputs. If there is no feedback on $\Delta\phi$ or Δf, the AFM system functions in the FM- or PM-AFM, respectively.

Theory of phase shift and frequency shift of hybrid PM/FM-AFM

Here, we theoretically consider the relationship between the tip–sample interaction force and the phase and frequency shifts of the cantilever, and we show that the operation by the hybrid PM/FM mode is possible. Following the procedure we previously demonstrated for the PM mode [20], we derive the relationship between the tip–sample interaction force and the phase and frequency shift of the cantilever. The motion of the oscillating cantilever can be expressed by the following equation:

$$m\ddot{z}(t)+\frac{2\pi f_0 m}{Q}\dot{z}(t)+kz(t)=F\cos(2\pi ft)+F_{ts} \quad (3)$$

Here, m, f_0 and f are the effective mass, the resonance frequency and the driving frequency of the cantilever, respectively. F and F_{ts} are the driving force of the cantilever and the tip–sample interaction force, respectively. The cantilever deflection signal $z(t)$ in the steady state is given by

$$z(t)=A_0\cos(2\pi ft+\phi) \quad (4)$$

where A_0 and ϕ are the amplitude of the oscillating cantilever and the phase difference between the driving and the deflection signals, respectively. By inserting Eq. (4) into Eq. (3), multiplying both sides of the resulting equation by $\cos(2\pi ft+\phi)$ and $\sin(2\pi ft+\phi)$ and then integrating over an oscillation period, one can obtain two general analytical relations for the phase shift as follows:

$$F\cos\phi=kA_0\left\{1-\left(\frac{f}{f_0}\right)^2\right\}-F_c \quad (5)$$

$$F\sin\phi=kA_0\frac{1}{Q}\left(\frac{f}{f_0}\right)-F_d \quad (6)$$

where F_c and F_d are the f components of the Fourier series for the conservative and dissipative tip–sample interaction forces, respectively, expressed as follows:

$$F_c=2f\int_0^{1/f}F_{ts}\cos(2\pi ft+\varphi)dt \quad (7)$$

$$F_d=2f\int_0^{1/f}F_{ts}\sin(2\pi ft+\varphi)dt \quad (8)$$

The phase shift $\Delta\phi$ of the cantilever is defined as the phase shift from the $-\pi/2$ phase delay of the cantilever oscillator signal as follows.

$$\Delta\phi=\phi-(-\pi/2) \quad (9)$$

On the basis of Eqs. (5), (6) and (9), $\Delta\phi$ is given by

$$\Delta\phi \approx \tan(\Delta\phi) = \frac{kA_0\left\{1-(f/f_0)^2\right\}-F_c}{kA_0(1/Q)(f/f_0)+F_d} \quad (10)$$

This equation indicates that the phase shift $\Delta\phi$ depends on both conservative force F_c and dissipative force F_d. From Eq. (10) and $f = f_0 + \Delta f$, the conservative force F_c is expressed as

$$F_c \approx -\left\{kA_0\frac{1}{Q}\left(1+\frac{\Delta f}{f_0}\right)+F_d\right\}\Delta\phi - 2kA_0\frac{\Delta f}{f_0} \quad (11)$$

In the PM mode, the cantilever is driven at a fixed resonant frequency f_0 ($\Delta f = 0$). In this case, the second term in Eq. (11) is zero, and assuming that the dissipative force is very small ($F_d \approx 0$), we find that the conservative force F_{cPM} is given only by the phase shift $\Delta\phi$ as follows:

$$F_{cPM} \approx -kA_0\frac{\Delta\phi}{Q} \quad (12)$$

In the FM mode, on the other hand, the cantilever is always driven at the resonance frequency ($\phi = -\pi/2$, $\Delta\phi = 0$). In this case, the first term in Eq. (11) is zero and the conservative force F_{cFM} is given only by the frequency shift Δf as follows:

$$F_{cFM} \approx -2kA_0\frac{\Delta f}{f_0} \quad (13)$$

By comparing Eq. (11) with Eqs. (12) and (13), we can obtain the following relationship

$$F_c \approx -kA_0\frac{\Delta\phi}{Q} - 2kA_0\frac{\Delta f}{f_0} \approx F_{c_{PM}} + F_{c_{FM}} \quad (14)$$

where the approximation $\Delta f/f_0 \ll 1$ is used. Equation (14) shows that the conservative force F_c is given by the two physical quantities of the oscillating cantilever: the phase shift $\Delta\phi$ and the frequency shift Δf. In other words, this equation means that it is possible to operate in the hybrid mode, which is a combination of PM and FM modes. Note that in the hybrid PM/FM mode, the set value of the phase shift feedback can be set to zero.

Next, let us consider how much faster the tip–sample interaction force can be measured by changing the FM mode to hybrid PM/FM mode. In the following, we will discuss high-speed AFM in FM mode using an algorithm based on the Fourier method in the PLL [16], instead of AFM in the FM mode using a lock-in amplifier in the PLL [15]. The Fourier method enables fast detection of the amplitude and phase of the cantilever displacement signal in a single period [16]. The demodulation of the frequency shift of the cantilever can be performed in a settling time of about 20 periods of the cantilever at minimum, assuming that the resonance frequency of the cantilever is 270 kHz [16]. Using an algorithm based on the Fourier method, the time constant τ_{PM} of the transient response of $\Delta\phi$ to the force changes is given by $\tau_{PM} = 1/f_0$ in the PM mode, while the time constant τ_{FM} of the transient response of Δf to the force changes is approximately given by $\tau_{FM} \approx 20/f_0$ in the FM mode. Thus, the time constant τ_{PM} is 1/20 of the time constant τ_{FM}. In Fig. 3, we show the qualitative transient responses of the feedback signals in the FM mode, the PM mode, and the hybrid-PM/FM-mode to the step. As in the FM mode, the feedback response of the tip-to-sample distance is slower, but in the hybrid-PM/FM-mode with a zero phase shift set point, the feedback response of the tip-to-sample distance is faster because the feedback response in the PM mode is added. By changing the FM mode to hybrid PM/FM mode, the transient response to force changes is expected to be reduced to about 1/20.

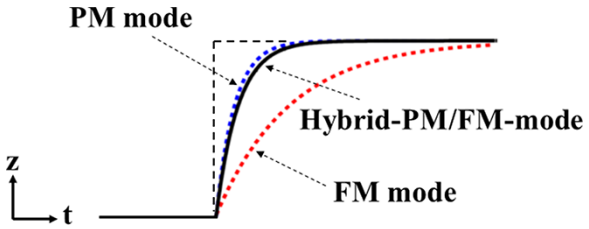

Fig. 3. Qualitative transient responses of the feedback signals to the step.

The minimum detectable force is a very important physical quantity that determines the spatial resolution of the AFM. The minimum detectable force is proportional to $B_{PM}{}^{0.5}$ in the PM mode [17,18], while it is proportional to $B_{FM}{}^{1.5}$ in the FM mode [26], where B_{PM} and B_{FM} are the bandwidths of the deflection sensor in PM and FM modes, respectively. When a wide bandwidth B_{PM} is used for high-speed scanning in the PM mode, the minimum detectable force increases rapidly. On the other hand, when a wide bandwidth B_{PM} is used for high-speed scanning in the PM mode, the minimum detectable force does not increase significantly. In hybrid PM/FM mode, the distance between the tip and the sample is controlled by the sum of the fast feedback signal with wide bandwidth B_{PM} for the phase shift and the slow feedback signal with narrow bandwidth B_{FM} for the frequency shift. By changing the FM mode to hybrid PM/FM mode, the minimum detectable force is mainly dominated by the wider bandwidth B_{PM} of the PM mode, allowing imaging with higher spatial resolution without increasing the minimum detectable force. Compared to the FM mode, the hybrid PM/FM mode has no spatial resolution limit and allows observation at atomic resolution.

These results suggest that the hybrid PM/FM mode is a new and very promising AFM operating mode that can significantly improve the PLL delay, which is a drawback in the FM mode, and increase the imaging speed of AFM systems operating in high-Q environments.

Experimental

Experiments were performed using a custom-built AFM system operating under ultrahigh-vacuum condition at room temperature. Deflection of the cantilevers was measured using the optical beam deflection method. The frequency and phase shifts of the oscillating cantilevers were measured by keeping the vibration amplitude (A) constant with the oscillation controller (OC4 oscillation controller, SPECS). The hybrid PM/FM-AFM image was obtained by adding the output signals of the two feedbacks (the feedback controller and the generic proportional and integral controller, SPECS). The percentages of signals added were 50% from one feedback loop and 50% from the other. The time constant for both feedbacks was 1.6 ms.

As sample surfaces, Si(111)-7 × 7 surface and diamond-(111) surfaces were used. The Si(111) surface was prepared by thermal treatment of a B-doped Si(111) sample. As the force sensors, we used Si cantilevers with a spring constant of $k = 26$ N/m, resonance frequency $f_0 = 242$–300 kHz and Q-factor of $Q = 3600$–8000. The vibration amplitude of the cantilever was $A = 10$ nm. Bias voltage between the tip and the surface was applied to compensate for the contact potential difference between the tip and the surface.

Results and discussion

By adding the feedback output from the PM mode to the feedback output from the FM mode, we experimentally investigated whether the hybrid PM/FM mode works stably and whether the hybrid PM/FM mode works more effectively than the FM mode.

Figure 4a and b shows AFM topographic and frequency shift error images of the Si(111) surface, respectively, measured in the FM mode. The AFM image in Fig. 4a was obtained from the feedback output that controls the tip-to-sample distance so that the frequency shift of the cantilever Δf is nearly constant. Here, the feedback conditions for this distance control were set such that the distance was slightly less controllable, resulting in a frequency shift error in the feedback as shown in Fig. 4b. In the AFM image in Fig. 4a, atomically flat terraces and steps on the Si surface are observed, but not clearly. In particular, the steps are blurry. The frequency shift error image in Fig. 4b shows that the frequency shift decreases sharply near the steps on the Si surface. It can also be seen that the frequency shift changes near the adsorbates on the terrace. In contrast, Fig. 4c shows an AFM image of the Si(111) surface measured in the hybrid PM/FM mode. The AFM image in Fig. 4c was obtained from the sum of two feedback outputs, one for the same feedback conditions for the frequency shift and the other for the strong feedback condition for the phase shift. In the AFM image in Fig. 4c, terraces and steps on the Si surface are clearly observed. In particular, adsorbates (bright spots) on the terraces and steps are very clearly observed. Comparing the cross-sectional profiles in Fig. 4d, e and f, it can be seen that the atomic level steps and their vicinities on the Si surface are clearly imaged in the hybrid PM/FM mode compared with the FM mode. Thus, we experimentally verified that the hybrid PM/FM mode, in which the feedback output of the PM mode is added to the feedback output of the FM mode, operates stably and enables the observation of atomic level features on the sample surface with high resolution.

Then, we compared the AFM topographic image obtained in the hybrid PM/FM mode with that obtained in the FM mode by increasing the scanning speed as much as possible (0.2 s/line) on the our AFM system. Figure 5a and b shows AFM images near the step on the diamond(111) surface measured in the FM and in the hybrid PM/FM modes, respectively. The AFM image in Fig. 5a was obtained from the feedback output that controls the tip-to-sample distance so that the frequency shift Δf is constant under strong feedback condition. The AFM image in Fig. 5b was obtained from the sum of feedback outputs that control the distance between the tip and the sample so that the phase shift $\Delta\phi$ is zero under strong feedback condition and feedback outputs that control the distance so that the time-averaged frequency shift $<\Delta f>$ is constant under weak feedback condition. Surface steps and terraces are clearly observed in both AFM images in Fig. 5a and b. Figure 5c and d shows the cross-sectional profiles along the white lines in Fig. 5a and b, respectively. In both FM and hybrid PM/FM modes, the cross-sectional profiles of the forward and backward scans are almost identical, indicating that the control of the tip–sample distance works well enough. Interestingly, the noise in the cross-sectional profiles in the hybrid PM/FM mode is much smaller than in the FM mode, about 1/5. By changing the FM mode to hybrid PM/FM

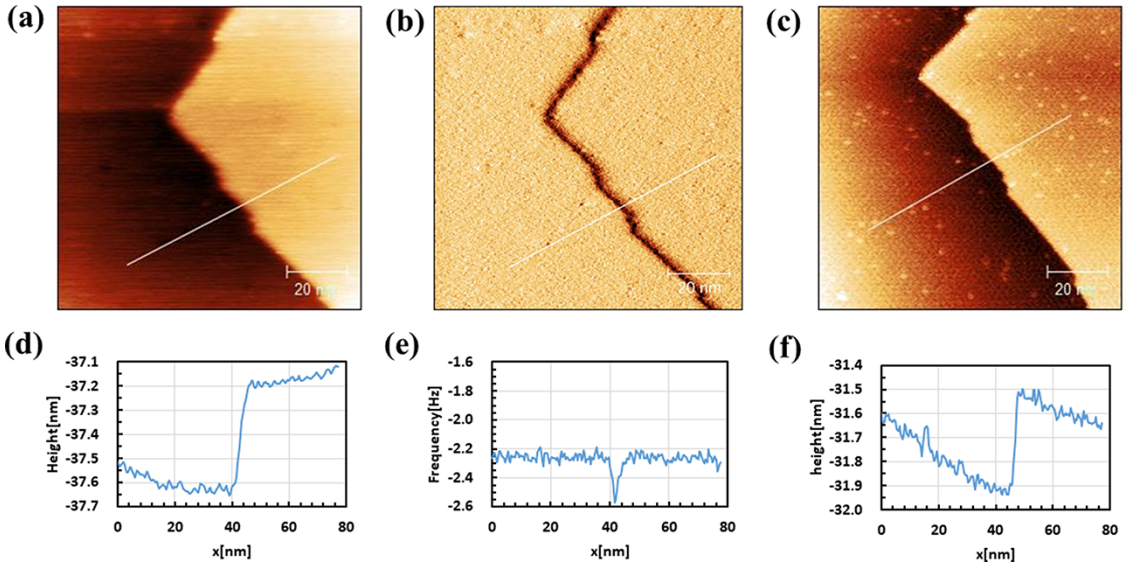

Fig. 4. (a) AFM topographic and (b) frequency shift error images of Si(111) surface obtained in the FM mode, (c) AFM topographic image of Si(111) surface obtained in the hybrid PM/FM mode. Cross-sectional profiles (d), (e) and (f) along the solid lines in images (a), (b) and (c), respectively. The spring constant, resonance frequency, Q-factor and vibration amplitude of the cantilever were $k = 26$ N/m, $f_0 = 242$ kHz, $Q = 3600$ and $A = 10$ nm, respectively. The averaged frequency shift of the cantilever was $\Delta f = -2.26$ Hz in (a) and (b), and the phase shift was $\Delta\phi = 0$ Hz in (c). The scanning area was 100 nm × 100 nm. The scanning speed was 1.5 s/line.

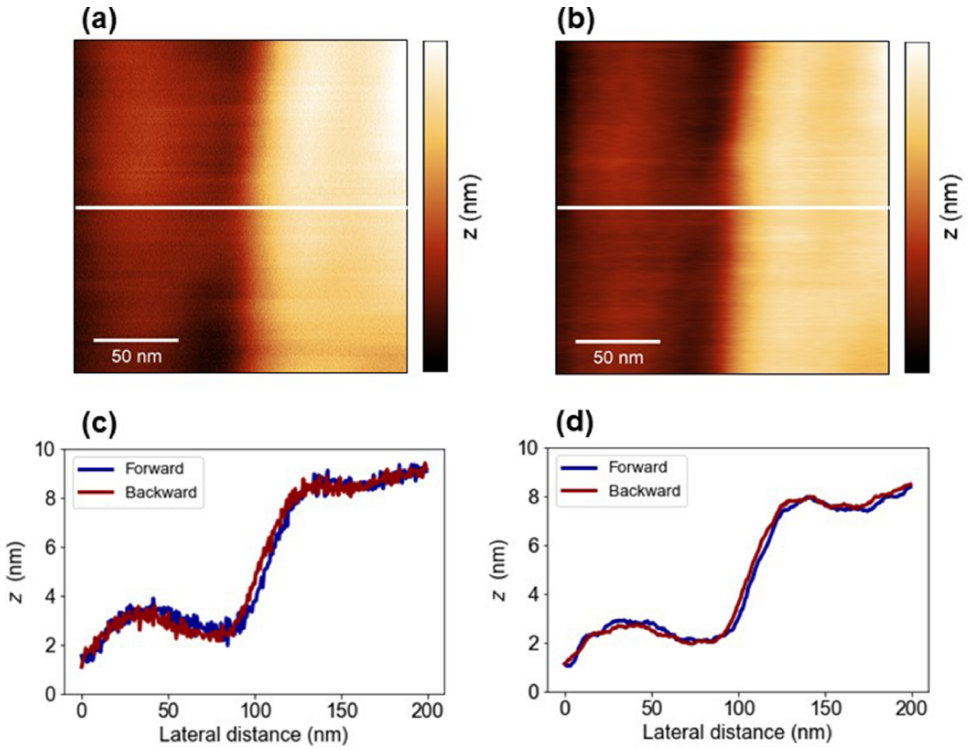

Fig. 5. (a) AFM topographic images of diamond surface obtained (a) in the FM and (b) the hybrid PM/FM modes, respectively. Cross-sectional profiles (c) and (d) along the solid lines in images (a) and (b), respectively. $k = 26$ N/m, $f_0 = 300$ kHz, $Q = 8000$ and $A = 10$ nm, respectively. The frequency shift of the cantilever was $\Delta f = -18$ Hz in (a), and the phase shift was $\Delta\phi = 0$ Hz in (b). The scanning area was 200 nm × 200 nm. The scanning speed was 0.2 s/line.

mode, the minimum detectable force is proportional to ${B_{\rm PM}}^{0.5}$ instead of ${B_{\rm FM}}^{1.5}$, which is in good agreement with the above prediction that the noise in AFM images will decrease. These results indicate that the hybrid PM/FM mode is a very promising mode of operation that can increase imaging speed and reduce noise compared to the FM mode.

To increase the imaging speed of hybrid PM/FM-AFM operating in a high-Q environment, it is necessary to increase the speed of various technological elements that make up an AFM system, for example, higher-frequency cantilevers, higher-bandwidth displacement sensors, faster frequency, amplitude and phase detection of cantilevers, wider bandwidth feedback circuits and faster scanners. In particular, AFM systems operating in a vacuum require the use of large, heavy specimen holders that enable heating and sputtering treatment of the specimen, making it difficult to increase scanner speed. In the future, the imaging speed of AFM systems operating in a high-Q environment could be further improved by replacing the scanner with a more rigid one with a higher resonant frequency.

Conclusion

We proposed the utilization of a hybrid technique of PM and FM modes to increase the imaging speed of AFM operating in high-Q environments. We theoretically investigated the performance of the hybrid PM/FM-AFM. We found the relationship between the phase shift, the frequency shift and the tip–sample interaction force from the equation of motion for the cantilever in high-Q environments. We found that the tip–sample conservative force is approximately given by the sum of the conservative force with respect to the phase shift in the PM mode and that with respect to the frequency shift in the FM mode. Preliminary experiments demonstrated that adding the feedback output of the phase shift from the PM mode to the feedback output of the frequency shift from the FM mode enables clearer imaging of atomic scale features on the Si surface.

Replacing the sample scanner with a more rigid one with a higher resonance frequency could further improve imaging speed, even for AFM systems operating in a high-Q environment. Hybrid PM/FM-AFM could also further improve imaging speed for FM-AFM systems, operating in low-Q environments, such as in gaseous or liquid environments.

Funding

JSPS KAKENHI Grant Numbers JP20K21128 and JP21H04662.

Acknowledgements

The authors thank T. Yamanaka and Z. Zhang for conducting the AFM experiments.

References

1. Zangwill A (1988) *Physics at Surfaces*, (Cambridge University Press, Cambridge).
2. Giessibl F J (1995) Atomic resolution of the silicon (111)-(7×7) surface by atomic force microscopy. *Science* 267: 68–71.
3. Sugawara Y, Ohta M, Ueyama H, and Morita S (1995) Defect motion on an InP(110) surface observed with noncontact atomic force microscopy. *Science* 270: 1646–1648.

4. Barth C and Reichling M (2002) Imaging the atomic arrangements on the high-temperature reconstructed α-Al_2O_3(0001) surface. *Nature* 414: 54–57.
5. Gross L, Mohn F, Moll N, Liljeroth P, and Meyer G (2009) The chemical structure of a molecule resolved by atomic force microscopy. *Science* 325: 1110–1114.
6. Kawai S, Foster A S, Canova F F, Onodera H, Kitamura S, and Meyer E (2014) Atom manipulation on an insulating surface at room temperature. *Nat. Commun.* 5: 4403.
7. Bamidele J, Lee S H, Kinoshita Y, Turanský R, Naitoh Y, Li Y J, Sugawara Y, Štich I, and Kantorovich L (2014) Vertical atomic manipulation with dynamic atomic-force microscopy without tip change via a multi-step mechanism. *Nat. Commun.* 5: 4476.
8. Naitoh Y, Turanský R, Brndiar J, Li Y J, Štich I, and Sugawara Y (2017) Subatomic-scale force vector mapping above a Ge(001) dimer using bimodal atomic force microscopy. *Nat Phys* 13: 663–667.
9. Adachi Y, Wen H F, Zhang Q Z, Miyazaki M, Sugawara Y, Sang H, Kantorovich L, Štich I, and Li Y J (2019) Tip-induced control of charge and molecular bonding of oxygen atoms on the rutile TiO 2 (110) surface with atomic force microscopy. *ACS Nano* 13: 6917–6924.
10. Ando T (2012) High-speed atomic force microscopy coming of age. *Nanotechnology* 23: 062001.
11. Miyata K, Tracey J, Miyazawa K, Haapasilta V, Spijker P, Kawagoe Y, Foster A S, Tsukamoto K, and Fukum T (2017) Dissolution processes at step edges of calcite in water investigated by high-speed frequency modulation atomic force microscopy and simulation. *Nano Lett.* 17: 4083–4089.
12. Kawai S and Kawakatsu H (2006) Atomically resolved amplitude modulation dynamic force microscopy with a high-frequency and high-quality factor cantilever. *Appl. Phys. Lett.* 89: 013108.
13. Dagdeviren O E, Götzen J, Hölscher H, Altman E I, and Schwarz U D (2016) Robust high-resolution imaging and quantitative force measurement with tuned-oscillator atomic force microscopy. *Nanotechnology* 27: 065703.
14. Albrecht T R, Grütter P, Horne D, and Ruger D (1991) Frequency modulation detection using high-Q cantilevers for enhanced force microscope sensitivity. *J. Appl. Phys.* 69: 668–673.
15. Dürig U, Steinauer H R, and Blanc N (1997) Dynamic force microscopy by means of the phase-controlled oscillator method. *J. Appl. Phys.* 81: 3641–3651.
16. Kokavecz J, Tóth Z, Horváth Z L, Heszler P, and Mechler Á (2006) Novel amplitude and frequency demodulation algorithm for a virtual dynamic atomic force microscope. *Nanotechnology* 17: S173–S177.
17. Kobayashi N, Li Y J, Naitoh Y, Kageshima M, and Sugawara Y (2006) High-sensitivity force detection by phase-modulation atomic force microscopy. *Jpn. J. Appl. Phys.* 45: L793–L795.
18. Fukuma T, Kilpatrick J I, and Jarvis S P (2006) Phase modulation atomic force microscope with true atomic resolution. *Rev. Sci. Instrum.* 77: 123703.
19. Sugawara Y, Kobayashi N, Kawakami M, Li Y J, Naitoh Y, and Kageshima M (2007) Elimination of instabilities in phase shift curves in phase-modulation atomic force microscopy in constant-amplitude mode. *Appl. Phys. Lett.* 90: 194104.
20. Kobayashi N, Li Y J, Naitoh Y, Kageshima M, and Sugawara Y (2008) Theoretical investigation on force sensitivity in Q-controlled phase-modulation atomic force microscopy in constant-amplitude mode. *J. Appl. Phys.* 103: 054305.
21. Li Y J, Kobayashi N, Nomura H, Naitoh Y, Kageshima M, and Sugawara Y (2008) High-speed phase-modulation atomic force microscopy in constant-amplitude mode capable of simultaneous measurement of topography and energy dissipation. *Jpn. J. Appl. Phys.* 47: 6121–6124.
22. Hölscher H (2008) Theory of phase-modulation atomic force microscopy with constant-oscillation amplitude. *J. Appl. Phys.* 103: 064317.
23. Van L P, Kyrylyuk V, Thoyer F, and Cousty J (2008) A stabler non contact atomic force microscopy imaging using a tuning fork for air and liquid environments: the zero phase mode atomic force microscopy. *J. Appl. Phys.* 104: 074303.
24. García R and Paulo A S (1999) Attractive and repulsive tip-sample interaction regimes in tapping-mode atomic force microscopy. *Phys. Rev. B* 60: 4961.
25. Aimé J P, Boisgard R, Nony L, and Couturier G (1999) Nonlinear dynamic behavior of an oscillating tip-microlever system and contrast at the atomic scale. *Phys. Rev. Lett.* 82: 3388.
26. Kobayashi K, Yamada H, and Matsushige K (2009) Frequency noise in frequency modulation atomic force microscopy. *Rev. Sci. Instrum.* 80: 043708.